Green Finance

https://www.aimspress.com/journal/GF

Green Finance, 6(4): 698–727.
DOI: 10.3934/GF.2024027
Received: 28 May 2024
Revised: 28 October 2024
Accepted: 13 November 2024
Published: 11 December 2024

Research article

Developing a machine learning model for fast economic optimization of solar power plants using the hybrid method of firefly and genetic algorithms, case study: optimizing solar thermal collector in Calgary, Alberta

Ali Omidkar, Razieh Es'haghian and Hua Song*

Chemical and Petroleum Engineering Department, Schulich School of Engineering, University of Calgary, Calgary, AB, Canada, T2N 4V8

Correspondence: Email: sonh@ucalgary.ca.

Abstract: Due to the depletion of fossil fuels and environmental concerns, renewable energy has become increasingly popular. Even so, the economic competitiveness and cost of energy in renewable systems remain a challenge. Optimization of renewable energy systems from an economic standpoint is important not only from the point of view of researchers but also industry owners, stakeholders, and governments. Solar collectors are one of the most optimized and developed renewable energy systems. However, due to the high degree of nonlinearity and many unknowns associated with these systems, optimizing them is an extremely time-consuming and expensive process. This study presents an economically optimal design platform for solar power plants with a fast response time using machine learning techniques. Compared with traditional mathematical optimization, the speed of economic optimization with the help of the machine learning method increased by up to 1100 times. A total of seven continuous variables and three discrete variables were selected for optimization of the parabolic trough solar collector. The objective functions were to optimize the exergy efficiency and the heat cost. As part of the environmental assessment, the cost of carbon dioxide emission was calculated based on the system's exergy and energy efficiencies. According to the sensitivity analysis, the mass flow of working fluid and the initial temperature of the fluid play the most significant roles. A simulated solar collector in Calgary was optimized in order to evaluate the applicability of the proposed platform.

Keywords: machine learning model; firefly optimization algorithm; solar collector

JEL Codes: C63

1. Introduction

It has recently been demonstrated that renewable energy is a viable alternative to fossil fuels in solving environmental problems and the energy crisis caused by conventional fuel use (Ashouri et al., 2015). This makes the use of renewable resources, such as solar energy, essential to promoting human sustainability and alleviating environmental concerns. One of the most effective measures to combat global warming has been the development of solar energy utilization. This type of energy, particularly in areas with higher average radiation levels, can reduce the consumption of fossil-based energy. As a result of new policies and government subsidies, the cost of utilizing solar energy has decreased, and installed capacity has increased. However, the proportion of this type of energy is still less than 3.6% despite all these worldwide initiatives (Pourasl et al., 2023). As a result of climate change, it appears that an increase in the proportion of solar energy is impossible unless government policies are changed in a paradigmatic manner.

Solar energy is a low-emission technology with a high potential for scaling up. It is therefore inevitable and necessary to increase the capacity of solar electricity to scales of terawatts in order to combat climate change. During the past few years, solar generation capacity has increased significantly, technology has improved, prices have decreased, and innovative business models have been developed to encourage the purchase of residential solar panels. However, further improvements are required in order to increase the share of solar energy at a price that is acceptable to society. Solar energy will only be able to fulfill this role if it is cost-competitive and cost-effective compared to fossil fuels, if carbon dioxide emissions are appropriately penalized, and if subsidies are likely to be significantly reduced (Sultan et al., 2020). Any new technology must be able to compete with existing commercially available technologies (Nguyen et al., 2023; Omidkar, Alagumalai, et al., 2024; Omidkar, Haddadian, et al., 2024; Omidkar et al., 2023). It has been proven that concentrated solar power (CSP) is an efficient technology for the production of clean and renewable energy. In essence, it works via focusing the sun's rays by using a reflective surface. There are two types of CSP systems: point focused and line focused. Parabolic dish collectors and solar towers are two types of point-focused collectors. There are two types of line-focused collectors: parabolic trough collectors (PTCs) and linear Fresnel reflectors (LFRs). Focus temperatures can reach over 1000 °C when using point-focused CSPs. At temperatures below 500 °C, line-focused CSP systems produce thermal and electrical energy (Cuce & Cuce, 2023; Cuce et al., 2021). PTC technology is widely regarded as the preferred CSP technology. As a stand-alone system, it can also be combined with other power generation systems to create hybrid systems. The nominal power produced by solar collectors directly correlates with radiation, so the determination of the geographical location is crucial. Furthermore, the average of sunny hours, wind speed, and humidity affect the performance of solar collectors. On the other hand, the performance of solar collectors can be described by the exergy conception, which means the maximum theoretical work obtainable from a given thermodynamic state when this reaches thermo-mechanical and chemical equilibrium with a reference state on environmental conditions entering a state called "dead state" (García-García et al., 2019). Cuse et al. designed a hybrid PTC/TEG energy system created with a thermoelectric generator (TEG) energy system (Cuce et al., 2024). They concluded that the overall thermal efficiency of PTC-TEG hybrid systems can be increased by 70% compared to PTC systems.

Elfeky and Wang (Elfeky & Wang, 2023) conducted techno-environ-economic assessment of two energy generation technologies, photovoltaic and CSP, in China and Egypt. According to their findings, establishing photovoltaic power plants in China is the best option, but concentrating on solar power plants in Egypt is the best option. The results show that in optimal conditions, a parabolic trough collector (PTC), which concentrates sunlight, produces 33.34% more electricity than a photovoltaic plant. Deai et al. introduced a PTC solar system using a micro-structured polymer foil. This system generates electricity through an organic Rankine cycle and produces freshwater using a multi-effect distillation process (Desai et al., 2021). The proposed system holds significant potential for regions facing electricity and water shortages. Using cyclopentane as the working fluid for the organic Rankine cycle, the plant achieved a levelized electricity cost of 0.116 EUR/kWh_e and a levelized water cost of 1.13 EUR/m^3 for Antofagasta, Chile, and 0.163 EUR/kWh_e and 1.62 EUR/m^3 for Cape Town, South Africa. Gilani and Hoseinzadeh conducted a comparative techno-economic analysis of compound parabolic collectors (CPC) in which all incident radiation is focused onto a receiver in solar water heating systems in the northern hemisphere (Azad Gilani & Hoseinzadeh, 2021). As a result of the study, CPCs are found to consume less auxiliary power in all selected locations than flat plate collectors. In all research conducted so far, optimizing design parameters, operational conditions, and input variables has remained a major challenge. Energy system efficiency can be affected by factors such as operational conditions, material properties, kind of collector and operating fluid, concentrating geometry, and cycle system (Mehdipour et al., 2020; Pal & K, 2021; Shafieian et al., 2020; Tabarhoseini et al., 2022). Myriads of studies have thus been conducted to determine the thermodynamic behavior of these systems using calculational models and predictive technologies like machine learning, specifically artificial neural networks (ANN) (Alawi, Kamar, Salih, et al., 2024; Brenner et al., 2023; Kottala et al., 2023; Mustafa et al., 2022; Ruiz-Moreno et al., 2022; Vakili & Salehi, 2023). Experiments in pilot plants are ineffective due to their high operational costs and time requirements. Neural network simulators offer the advantages of simplicity, speed, and the ability to handle nonlinear and complex interactions between inputs and variables, making them a promising solution for complex data analyses. (Haykin, 1998). A common method of solving multi-objective optimization problems (MOPs) is to use evolutionary algorithms (EAs), such as genetic algorithms and particle swarm algorithms. Following the development of swarm intelligence (SI) algorithms, particle swarm algorithms expanded into multi-objective particle swarm optimization algorithms (MOSPO). A number of studies have attempted to utilize ANNs in addition to other concepts for evaluating renewable energy systems; however, the number of studies is limited. Recently, there has been a surge in interest in employing artificial intelligence techniques to optimize and predict renewable energy production systems (Elsheikh et al., 2024; Shboul et al., 2024; Shboul et al., 2024; Zayed et al., 2023a; Zayed et al., 2023b; Zayed et al., 2021). Other challenges include high CPU usage, optimization, and interpretation. The knowledge gap that motivated this study is illustrated in Table 1.

Table 1. Illustration of the knowledge gap and comparison of this study with the literature review. * means that the study contains the feature; – means that the study lacks the feature.

Ref. and year	Method	MI optimization	TEA	LCA	Applicability of other problems
(Salari et al., 2024), 2024	Heat transfer	*	-	-	-
(Alawi, Kamar, Abdelrazek, et al., 2024), 2024	Heat transfer	*	-	-	-
(Wu et al., 2022)	Linear regression	*	-	-	-
(Wang et al., 2021), 2021	ANN	*	-	-	-
This study	Thermodynamic and heat transfer	*	*	*	*

To overcome these challenges and to be useful in industrial settings, a supervised machine-learning approach has been developed in this study. The purpose of this study is to optimize energy, exergy, heat cost, and carbon dioxide emission costs for a complex renewable energy system using a machine-learning approach.

2. Methods

2.1. System description

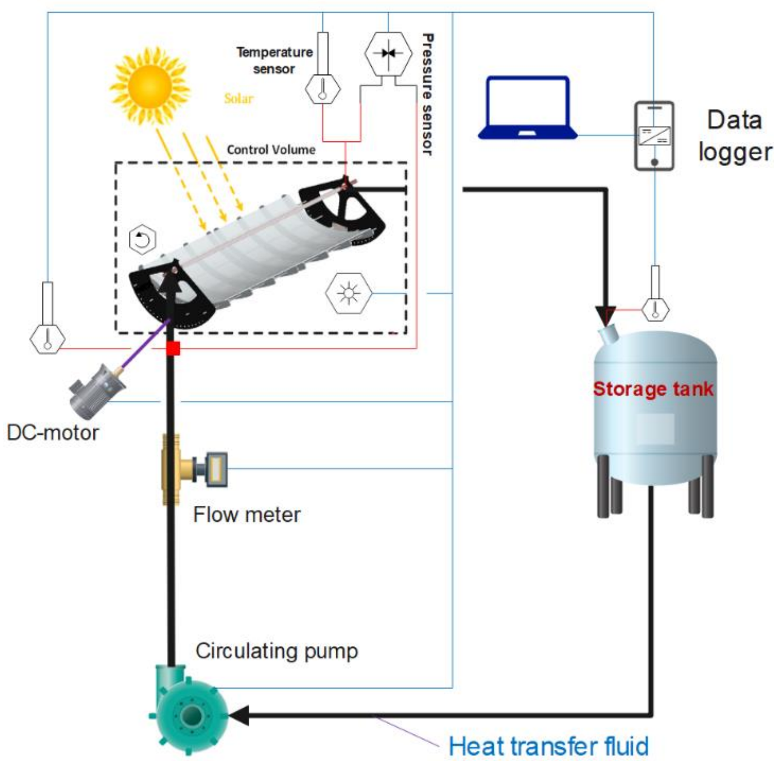

Figure 1. Schematic view of the parabolic trough solar collector system.

The system used in this study is depicted in Figure 1. The components of the parabolic trough solar collector are a parabolic collector, pump, storage tank or thermal heat exchanger, flow transducer, DC motor, piping, working fluid, pressure and temperature sensors, CPU, and data storage. Through an absorb tube, the working fluid receives heat and enters the storage tank at a high temperature. Energy from the storage tank can be used simultaneously or whenever needed. It is also possible to use the storage tank to supply the energy of another working fluid via a heat exchanger for other applications such as the Rankine cycle, absorption refrigeration cycle, or the supply of hot water for residential use. CPUs can utilize the thermal and hydrodynamic properties of working fluids and receive atmospheric conditions from sensors. The system can also be optimized by using the aforementioned parameters, the mass flow of the working fluid, and the angle of the reflector.

2.2. Governing equations

The difference between solar time and local time can be derived via Equation (1) (Duffie et al., 2020).

$$T_{st}-T_{lt}=4\times\left(L_{loc}-L_{st}\right)+E \quad (1)$$

$$E=229.2\times\begin{pmatrix}0.000075+0.001868\,\mathrm{Cos}\,\beta-0.032077\,\mathrm{Sin}\,\beta\\-0.014615\,\mathrm{Cos}\,2\beta-0.04089\,\mathrm{Sin}\,2\beta\end{pmatrix} \quad (2)$$

In Equation (2), the $\beta=\frac{360\left(n-1\right)}{365}$ and the n is the n^{th} day of the year.

The angle of sunset can be calculated using Equation (3), in which φ and δ are the latitude and deviation angle, respectively (Duffie et al., 2020).

$$\omega=\mathrm{Cos}^{-1}\left(-\tan\varphi\times\tan\delta\right) \quad (3)$$

$$\delta=23.45\sin\left(\frac{360\left(284+n\right)}{365}\right) \quad (4)$$

The pressure drop inside the absorber tube can be calculated by Equation (5).

$$\Delta P=f_{Darcy}\frac{V_1^2L}{2gD_2} \quad (5)$$

$$V_1=\frac{4\dot{m}}{\rho\pi D_2^2} \quad (6)$$

In Equations (5) and (6), ΔP is pressure loss along the length of L in the pipe, D_2 is the inner diameter of the absorber pipe, g is the gravitational acceleration, V_1 is the average velocity of fluid inside the pipe, $\dot{m}$ is mass flow, and ρ is the density of the fluid. Depending on the laminar or turbulent flow regime, f_{Darcy} can be derived using Equations (7) or (8), in which f is the friction factor and ε is the pipe's effective roughness height.

$$\text{Laminar flow: } f_{Darcy} = \frac{64}{\mathrm{Re}_{D_2}} \tag{7}$$

$$\text{Turbulent flow: } f = \frac{f_{Darcy}}{4}$$

$$\frac{1}{\sqrt{f}} = -2\log\left(\frac{\frac{\varepsilon}{D_2}}{3.7} + \frac{2.51}{\mathrm{Re}_{D_2}\sqrt{f}}\right) \tag{8}$$

Based on Figure 2, the energy balance in one element of the tube in which the temperature gradient is linear can be established using the system of Equations (9–13).

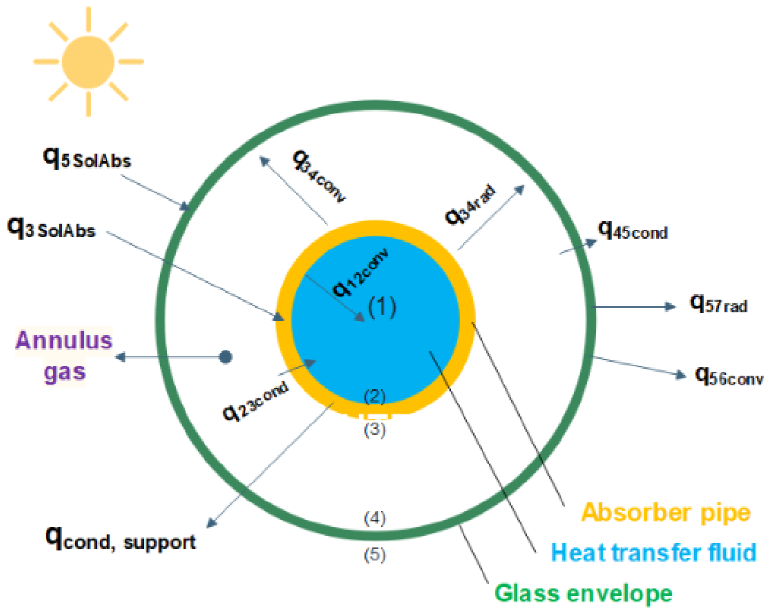

Figure 2. Heat flux in one element of the parabolic trough solar collector. $q_{1\text{-}2,\ conv}$: convection heat transfer between the inner surface of the absorber tube and working fluid. $q_{2\text{-}3,\ cond}$: conduction heat transfer between the outer and inner surfaces of the absorber tube. $q_{5solabs}$: solar irradiation absorption from the incident solar irradiation to the outer glass envelope surface. $q_{3solabs}$: solar irradiation absorption from the incident solar irradiation to the outer surface of the absorber tube. $q_{4\text{-}2,\ conv}$: convection heat transfer from the absorber tube outer surface to the envelope inner surface. $q_{4\text{-}2,\ rad}$: radiation heat transfer from the absorber tube outer surface to the envelope inner surface. $q_{4\text{-}5,\ cond}$: conduction heat transfer from the envelope's inner surface to the envelope's outer surface. $q_{5\text{-}6,\ conv}$: convection heat transfer from the envelope's outer surface to the atmosphere. $q_{5\text{-}7,\ rad}$: radiation heat transfer from the envelope's outer surface to the sky.

$$\dot{q}'_{12,conv} = \dot{m}c\left(T_{outlet} - T_{inlet}\right) \tag{9}$$

$$\dot{q}'_{12,conv} = \dot{q}'_{23,cond} \tag{10}$$

$$\dot{q}'_{3,SolAbs} = \dot{q}'_{34,conv} + \dot{q}'_{34,rad} + \dot{q}'_{23,cond} + \dot{q}'_{cond,bracket} \tag{11}$$

$$\dot{q}'_{34,conv} + \dot{q}'_{34,rad} = \dot{q}'_{45,cond} \tag{12}$$

$$\dot{q}'_{45,cond} + \dot{q}'_{5,Soldos} = \dot{q}'_{56,conv} + \dot{q}'_{57,rad} \tag{13}$$

In the energy conservation system of equations, $\dot{q}'_{12,conv}$ is the convection heat transfer between the absorber tube's inner surface and working fluid derived by Equations (14) and (15) (Bergman, 2011; Gnielinski, 1976; Jehring, 1992). h_1 is the convection heat transfer coefficient of fluid at T_1, D_2 is the inner diameter of the absorber tube, T_2 is the temperature of the absorber tube's inner surface, T_1 is the temperature of working fluid, and Nu_{D2} is the Nusselt number based on D_2 and k_1. Depending on the flow regime (laminar, transient, and turbulent), the Nusselt number can be derived.

$$\begin{gathered} \dot{q}'_{12,conv} = h_1 D_2 \pi \left(T_2 - T_1\right) \\ h_1 = Nu_{D_2} \frac{k_1}{D_2} \\ \text{Laminar flow: } Nu = 4.36 \end{gathered} \tag{14}$$

$$\text{For transient and turbulent flow: } Nu_{D_2} = \frac{\frac{f_2}{8}\left(\mathrm{Re}_{D_2} - 1000\right)\mathrm{Pr}_1}{1 + 12.7\sqrt{\frac{f_2}{8}}\left(\mathrm{Pr}_1^{\frac{2}{3}} - 1\right)}\left(\frac{\mathrm{Pr}_1}{\mathrm{Pr}_2}\right)^{0.11} \tag{15}$$

$$f_2 = \left(1.82\log\left(\mathrm{Re}_{D_2}\right) - 1.64\right)^{-2}$$

Between the inner and outer surfaces of the absorber pipe, the mechanism of heat transfer is based on Equation (16). k_{23} is the conduction heat transfer coefficient of the absorber tube, T_3 is the outer surface temperature of the absorber tube, and D_3 is the outer diameter of the absorber tube.

$$\dot{q}'_{23,cond} = \frac{2\pi k_{23}}{\ln\frac{D_3}{D_2}}\left(T_2 - T_3\right) \tag{16}$$

Heat transfer mechanisms can vary depending on the pressure between the envelope cover (mostly made of glass) and the absorber tube. Heat is transferred between the envelope and the absorber tube by free molecular convection when the pressure is lower than 1 Torr. When the pressure exceeds 1 Torr, the heat transfer mechanism becomes natural convection.

Pressure lower than 1 Torr

$$\dot{q}'_{34,conv} = \pi D_3 h_{34} \left(T_3 - T_4\right)$$

$$h_{34} = \frac{k_{std}}{\frac{D_3}{2\ln\frac{D_4}{D_3}} + b\lambda\left(\frac{D_3}{D_4}+1\right)}$$

$$b = \frac{\left(2-a\right)\left(9\gamma-5\right)}{2a\left(\gamma+1\right)} \tag{17}$$

$$\lambda = \frac{2.331\times10^{-20}\left(T_{34}+273.15\right)}{P_a\delta^2}$$

Pressure higher than 1 Torr

$$\dot{q}'_{34,conv} = \frac{2.425k_{34}\left(T_3-T_4\right)\left(\frac{\Pr Ra_{D_3}}{0.861+\Pr_{34}}\right)^{\frac{1}{4}}}{\left(1+\left(\frac{D_3}{D_4}\right)^{\frac{3}{5}}\right)^{\frac{5}{4}}} \tag{18}$$

$$Ra_{D_3} = \frac{g\beta\left(T_3-T_4\right)D_3^3}{\alpha\nu}$$

$$\beta = \frac{1}{T_{avg}}$$

D_3 is the inner diameter of the envelope, D_4 is the diameter of the outer surface of the envelope, h_{34} is the convection heat transfer coefficient at the average temperature T_{34}, T_4 is the inner temperature of the envelope, and k_{std} is the conduction heat transfer of the gas. b is the interaction factor, λ is the mean free path, a is a correlation factor, γ is the ratio of specific heats of the gas, T_{34} is the average temperature, P_a is the pressure of the gas inside the envelope (mmHg), and δ is the molecular diameter of the gas. For the equation related to the higher pressure, Pr_{34} is the Prandtl number, Ra_{D3} is the Rayleigh number, and β is the thermal expansion coefficient of the gas.

The heat transfer mechanism between the absorber tube and the envelope is radiation, which can be derived via Equation (19). σ is the Stefan- Boltzmann constant, ε_3 is the emissivity coefficient of the absorber, and ε_4 is the emissivity coefficient of the envelope.

$$\dot{q}'_{34,rad} = \frac{\sigma\pi D_3\left(T_3^4-T_4^4\right)}{\left(\frac{1}{\varepsilon_3}+\left(1-\varepsilon_4\right)\frac{D_3}{\varepsilon_4 D_4}\right)} \tag{19}$$

The conduction heat transfer in the envelope is similar to the conduction heat transfer in the absorber tube [Equation (16)].

There are two mechanisms for heat transfer between the atmosphere and the envelope: convection and radiation. Depending on the wind speed, convection can be natural or forced. The radiation heat loss exists due to the temperature difference between the envelope and the sky. The convection heat transfer between the envelope and the atmosphere is the main resource for heat loss, specifically when there is wind. T_5 is the outer temperature of the envelope, T_6 is the atmospheric temperature, h_{56} is the convection heat transfer coefficient of the air at the average temperature, k is the conduction heat transfer coefficient at the average temperature, D_5 is the outer diameter of the envelope, and Nu_{D5} is the Nusselt number based on the outer diameter of the envelope.

$$\begin{aligned} \dot{q}'_{56,conv} &= h_{56}\pi D_5 \left(T_5 - T_6\right) \\ h_{56} &= \frac{k_{56}}{D_5} Nu_{D_5} \end{aligned} \tag{20}$$

If there is no wind (wind speed lower than 0.1 m/s), the heat transfer mechanism between the envelope and the atmosphere is natural convection.

$$\begin{aligned} \bar{N}u_{D_5} &= \left[0.6 + \frac{0.387 Ra_{D_5}^{\frac{1}{6}}}{\left[1 + \left(\frac{0.559}{\Pr_{56}} \right)^{\frac{9}{16}} \right]^{\frac{\beta}{27}}} \right]^2 \\ Ra_{D_5} &= \frac{g\beta \left(T_5 - T_6\right) D_5^3}{\alpha_{56} \nu_{56}} \\ \beta &= \frac{1}{T_{56}} \\ \Pr_{56} &= \frac{\nu_{56}}{\alpha_{56}} \end{aligned} \tag{21}$$

Ra_{D5} is the Rayleigh number for the air based on the outer diameter of the envelope, g is the gravitational acceleration, α_{56} is the thermal diffusivity of the air at T_{56}, β is the volumetric expansion coefficient for an ideal gas, Pr_{56} is the Prandtl number for the air at temperature T_{56}, ν_{56} is the kinematic viscosity of the air and temperature T_{56}, and T_{56} is the average temperature of the film. If the wind speed becomes higher than 0.1 m/s, the heat transfer between the envelope and atmosphere is forced convection.

$$\begin{aligned} &\bar{N}u_{D_5} = C \,\mathrm{Re}_{D_5}^m \Pr_6^n \left(\frac{\Pr_6}{\Pr_5} \right)^{\frac{1}{4}} \\ &\begin{cases} 1 < \mathrm{Re}_D < 40: \ C = 0.75, \ \ m = 0.4 \\ 40 < \mathrm{Re}_D < 1000: \ C = 0.51, \ \ m = 0.5 \\ 1000 < \mathrm{Re}_D < 200000: \ C = 0.26, \ \ m = 0.6 \\ 200000 < \mathrm{Re}_D < 1000000: \ C = 0.076, \ \ m = 0.7 \end{cases} \end{aligned} \tag{22}$$

The radiation heat transfer between the envelope and the sky because of the temperature difference between the outer surface of the envelope and the sky can be derived from Equation (23).

$$\dot{q}'_{57,rad} = \sigma D_5 \pi \varepsilon_5 \left(T_5^4 - T_7^4\right) \tag{23}$$

ε_5 and T_7 are the emissivity of the outer surface of the envelope and sky temperature, respectively. Generally, the sky temperature is 8 °C lower than the atmospheric temperature.

The absorption of sunlight can be derived by Equation (24).

$$\begin{aligned} &\dot{q}'_{5,SolAbs} = \dot{q}'_{si}\eta_{env}\alpha_{env} \\ &\eta_{env} = \varepsilon'_1\varepsilon'_2\varepsilon'_3\varepsilon'_4\varepsilon'_5\varepsilon'_6\rho_{cl}K \\ &K = \cos\theta + 0.000884\theta - 0.00005369\theta^2 \end{aligned} \tag{24}$$

$\dot{q}'_{si}$ is the radiation of light along the receiver, η_{env} is the light efficiency of the envelope, and α_{env} is the absorption of the envelope. ε'_1 is the collector's shadow, ε'_2 is the localization error, ε'_3 is the geometry error, ε'_4 is the fouling on the mirrors, ε'_5 is the fouling on the collectors, ε'_6 is the unconsidered error, and ρ_{cl} is the reflection factor of the clean mirror. The factor K is the correction factor of the light angle, and θ is the deviation angle of the solar collector.

The light absorption in the absorber tube can be derived from Equation (25).

$$\begin{aligned} &\dot{q}'_{3,SolAbs} = \dot{q}'_{si}\eta_{abs}\alpha_{abs} \\ &\eta_{abs} = \eta_{env}\tau_{env} \end{aligned} \tag{25}$$

η_{abs} is the light efficiency in the absorber tube, α_{abs} is the absorption coefficient of the absorber tube, and τ_{env} is the light transmission coefficient in the envelope.

The envelope and the absorber tube at the focal length of the solar collector are maintained by the supporters. Generally, at the end of each solar element, there is one supporter every 4 m. The heat loss, assuming the support bracket behaves as an infinite fin with a temperature 10 °C lower than T_3, can be derived from Equation (26):

$$\dot{q}'_{bracket,cond} = \sqrt{\bar{h}_b P_b k_b A_{cs,b}}\,\frac{\left(T_{base} - T_6\right)}{L_{HCE}} \tag{26}$$

In Equation (26), $\bar{h}_b$ is the convection heat transfer of the supporter, which depends on the wind speed, P_b is the perimeter of the supporter, k_b is the conduction heat transfer coefficient, $A_{cs,b}$ is the area of the cross-section of the bracket, T_{base} is the base temperature of the bracket supporter, T_6 is the atmospheric temperature, and L_{HCE} is the length of the solar collector.

2.3. Exergy analysis

By applying the second law of thermodynamics to the control volume of the solar collector, Equation (27) is obtained:

$$\dot{E}x_{f,in} + \dot{E}x_s = \dot{E}x_{f,out} + \dot{E}x_l + \dot{E}x_{des} \tag{27}$$

$\dot{E}x_{f,in}$ is the inflow of exergy to the fluid, $\dot{E}x_s$ is the inflow of exergy from sunlight, $\dot{E}x_{f,out}$ is the outflow of exergy of the fluid, $\dot{E}x_l$ is the exergy loss, and $\dot{E}x_{des}$ is the exergy destruction. The exergy of the sunlight can be calculated using (Landsberg & Mallinson, 1976). T_{sun} is the surface temperature of the sun (5780 K), and l is the interaction factor. f_H is the view factor, which explains the geometry correlation between the radiation source and the receiver, ε_H is the dilution factor, and f_r is the geometry factor of reflection by the absorber.

$$\begin{aligned} \dot{E}x_s &= \dot{Q}_s \times a\left(1-\frac{4}{3}\times\left(\frac{T_{amb}}{T_{sun}\times l}\right)+\frac{1}{3}\times\left(\frac{T_{amb}}{T_{sun}\times l}\right)^4\right) \\ l &= \left(\frac{f_H \varepsilon_H \alpha}{f_r \varepsilon_r}\right)^{0.25} \end{aligned} \tag{28}$$

The useful exergy is defined as the difference between the inflow exergy and the outflow exergy of the fluid (Badescu, 2018).

$$\dot{E}x_u = \dot{E}x_{f,out} - \dot{E}x_{f,in} = \dot{Q}_u - \dot{m}_f C_p T_{amb} \ln\left(\frac{T_{out}}{T_{in}}\right) - \dot{m}_f T_{amb} \frac{\Delta P}{\rho_f T_f} \tag{29}$$

The exergy loss can be calculated using Equation (30) (Bellos & Tzivanidis, 2017). $\dot{E}x_{l,opt}$ is light exergy loss and $\dot{E}x_{l,thermal}$ is the thermal exergy loss.

$$\begin{aligned} \dot{E}x_l &= \dot{E}x_{l,opt} + \dot{E}x_{l,thermal} \\ \dot{E}x_{l,opt} &= \left(1-\eta_{opt}\right)\times \dot{E}x_s \\ \dot{E}x_{l,thermal} &= \dot{Q}_l\left(1-\frac{T_{amb}}{T_r}\right) \end{aligned} \tag{30}$$

The exergy destruction shows irreversibility due to heat loss. Specifically, this parameter defines a probable work that disappears when there is thermal energy flow between hot and cold sources. The exergy destruction can be derived using Equation (31) (Kalogirou, 2004). In the solar collector, exergy destruction can occur mainly from two sources: between the absorber tube and the sun and between the absorber tube and the working fluid.

$$\begin{aligned} \dot{E}x_{des} &= \dot{E}x_{des,s\to r} + \dot{E}x_{des,r\to f} \\ \dot{E}x_{des,s\to r} &= \left(1-\eta_{opt}\right)\times \dot{E}x_s - Q_{abs}\times\left(1-\frac{T_{amb}}{T_r}\right) \\ \dot{E}x_{des,r\to f} &= \dot{Q}_u \times\left(1-\frac{T_{amb}}{T_r}\right) - \dot{E}x_u \end{aligned} \tag{31}$$

Exergy efficiency can be calculated using Equation (32).

$$\eta_{exergy} = \frac{\dot{E}x_u}{\dot{E}x_s} \tag{32}$$

2.4. Economical modeling

The net price cost of the solar collector can be calculated as Equation (33). The CRF is the capital recovery factor, $C_{O\&M}$ is the operational and maintenance cost (which is considered as 2% of capital investment), C_s is the capital investment, i is the interest rate (4%), and n is the total operational years (Frangopoulos, 1987). C_H is the cost of heat production by the collector, N is the total annual operational hours, and q_u is the efficient heat transfer to the working fluid.

$$\begin{aligned} NPC &= CRF \times \left(C_{O\&M} + C_s\right) \\ CRF &= \frac{(1+i)^n}{(1+i)^n - 1} \\ C_H &= \frac{NPC}{q_u \times N} \end{aligned} \tag{33}$$

The purchase cost of various components of solar collectors can be found in Table 2.

Table 2. Purchase cost of each component of a solar collector.

Component	Unit	Cost
Solar collector	$/m^2	266.7
Working fluid	$/lit	7.4
Storage tank	$/m^3	44
Pump	$/kW	2100

2.5. Energy-environment analysis

The environmental emission of a solar collector system can be derived using Equation (34) (Faizal et al., 2015).

$$x_{CO_2,eq} = y_{CO_2,eq} \times \dot{Q}_u \times t_{operational} \tag{34}$$

$x_{CO_2,eq}$ is the equivalent emitted CO_2 during the operational time of $t_{operational}$, $y_{CO_2,eq}$ is the emitted CO_2 of the reference boundary control system, which is calculated using life cycle assessment methods, and $\dot{Q}_u$ is the produced power of the reference boundary system.

2.6. Exergy-environment analysis

Environmental assessment can also be carried out by another method. In this kind of assessment, which is similar to that of section 2.5, instead of power, the amount of exergy inside the system will be taken into account. This method is more conservative and accurate than energy-environment analysis.

$$x_{CO_2,eq} = y_{CO_2,eq} \times \dot{E}x_u \times t_{operational} \tag{35}$$

2.7. Energy-environment-economy analysis

According to (Deniz & Çınar, 2016), the economic effects of producing carbon dioxide can be derived from Equation (36). C_{CO2} is the economic-environmental parameter of the system, and c_{CO2} is the cost of carbon dioxide production. It is possible to prevent climate change and other phenomena such as global warming by reducing carbon dioxide emissions as much as possible. By employing a conservative approach, the carbon emission cost method aims to provide a more tangible view of the environmental impacts. By formulating incentives and punishment policies, this method seeks to reduce the environmental impact of energy systems.

$$C_{CO_2} = x_{CO_2} \times c_{CO_2} \tag{36}$$

2.8. Machine learning method: Support vector regression

The support vector regression technique follows the principle of structural risk minimization and has been successfully applied to data classification, regression, and nonlinear systems modeling (Vapnik, 1999). In a regression model with a training set $G = \{(x_i, y_i)\}_i^n \subset R^d \times R$, in which x_i and y_i are the input and output variables, respectively, of i^{th} pair of datasets, and n indicates the total number of datasets, the SVR is a kernel method that performs the nonlinear regression using a kernel trick. The kernel-induced feature space F is used to perform linear regression on each input $x_i \in R^d$ via a nonlinear feature map $\phi(\bullet)$. For all training data, SVR aims to find a function that has minimum deviation ε from the actual target y_i. Deviations greater than ε are not accepted. Accordingly, SVR considers the following linear estimation function in order to achieve the stated objective:

$$\begin{aligned} &f(x) = \omega\phi(x) + b \\ &\phi : R^n \to F, \quad \omega \in F \end{aligned} \tag{37}$$

In Equation (37), ω and b are coefficients and $\phi(x)$ indicates the high-dimensional feature space that is nonlinearly mapped from the input space x. The coefficients w and b can be estimated by minimizing the regularized risk function.

$$\begin{aligned} &R(f) = C\frac{1}{n}\sum_{i-1}^{n} L_\varepsilon\left(f(x_i) - y_i\right) + \frac{1}{2}\|\omega\|^2 \\ &L\left(f(x,y)\right) = \begin{cases} |f(x) - y| - \varepsilon & |f(x) - y| \geq 0 \\ 0 & \text{otherwise} \end{cases} \end{aligned} \tag{38}$$

In Equation (38), $\frac{\|\omega^2\|}{2}$ is the Euclidean norm; this parameter is used to estimate the flatness of the function. This feature is used to avoid over-fitting. The difference between measured values and values calculated by the regression function is shown by ε. It is possible to visualize this difference as a tube surrounding the regression function. The parameter C represents the cost function measuring empirical risk; it is used to determine the trade-off between empirical risk and model flatness. In this context, $C > 0$ represents the penalty degree of the sample with error exceeding ε. The loss function

$L_\varepsilon\left(f\left(x_i\right)-y_i\right)$ is referred to as the ε-insensitive loss function. In the empirical analysis, C and ε are parameters that are defined by the user.

Overall, SVR is a versatile and powerful tool for regression tasks, especially when dealing with nonlinear data and high-dimensional feature spaces. However, the choice of the machine learning method should always be guided by the specific characteristics of the dataset and the problem at hand.

Statistical parameters are used to evaluate the performance of the SVR model for the training and testing sets: the coefficient of determination (*R2*), mean absolute error (MAE), root mean square error (RMSE), and mean squared error (MSE).

$$R^2 = 1 - \frac{\sum_{i=1}^{N}\left(Y_i^{\exp} - Y_i^{pred}\right)^2}{\sum_{i=1}^{N}\left(Y_i^{\exp} - \bar{Y}^{\exp}\right)^2} \tag{39}$$

$$MAE = \frac{1}{N}\sum_{i=1}^{N}\left|Y_i^{\exp} - Y_i^{pred}\right| \tag{40}$$

$$RMSE = \sqrt{\frac{1}{N}\sum_{i=1}^{N}\left(Y_i^{\exp} - Y_i^{pred}\right)^2} \tag{41}$$

$$MSE = \frac{1}{N}\sum_{i=1}^{N}\left(Y_i^{\exp} - Y_i^{pred}\right)^2 \tag{42}$$

2.9. Firefly opt imization algorithm

An optimization algorithm based on the flashing behavior of fireflies is called the firefly algorithm (FA). Bioluminescence is used by fireflies to communicate and attract mates. In order to optimize solutions to various optimization problems, the algorithm simulates this behavior. As a result of this knowledge, we can idealize some of the flashing characteristics of fireflies in order to develop algorithms that are inspired by fireflies. The FA is described by the following rules:

- Since fireflies are unisex, one firefly will be attracted to another firefly regardless of their gender.
- The attractiveness of a firefly is directly proportional to its brightness. Consequently, if there are two flashing fireflies, the less bright one will move toward the brighter one. There is a direct relationship between attractiveness and brightness, both of which decrease as their distance increases. A firefly will move randomly if there is no other that is brighter.
- Fireflies' brightness is affected or determined by the objective function's landscape.

The FA is a relatively simple, yet effective, optimization algorithm that has gained significant attention due to its ease of implementation and strong global exploration capabilities. The algorithm's inherent ability to thoroughly search the solution space reduces the likelihood of becoming trapped in local optima. Its adaptability to various problem types, including continuous, discrete, and multi-objective optimization, further enhances its versatility. Furthermore, FA's parallel processing nature can significantly accelerate the optimization process. Its robustness to dynamic and noisy environments makes it well-suited for real-world applications.

Compared to other metaheuristic algorithms, FA offers several advantages. Unlike genetic algorithms (GA), FA relies on a more straightforward attraction mechanism, which can lead to faster convergence. While simulated annealing (SA) explores the solution space sequentially, FA's simultaneous exploration of multiple solutions can potentially accelerate the search process. Additionally, FA's independence from pheromone-based information reduces computational overhead and simplifies implementation. Its suitability for non-differentiable, complex, and multi-modal functions further underscores its versatility.

More information about this method and pseudo code is available in (Fister et al., 2013; Johari et al., 2013; Yang, 2010).

2.10. Research methodology

The research methodology is illustrated in Figure 3. Initially, a dataset is produced using input variables and solving the governing equations mentioned in previous sections. The produced dataset is used for training the SVR model. Then, the SVR model is optimized by the firefly optimization method to maximize accuracy. Then, this model is used by the genetic algorithm (GA) for the optimization of design parameters.

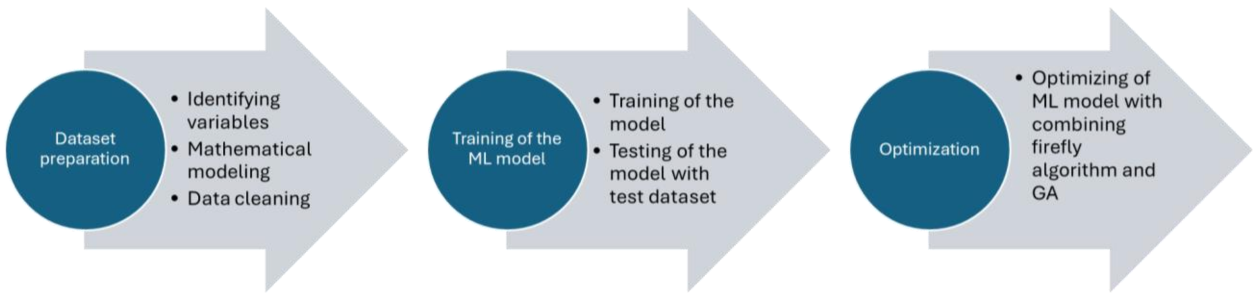

Figure 3. Schematic of research methodology.

The FA and GA are metaheuristic optimization algorithms that offer complementary strengths. FA excels in global exploration, efficiently traversing the search space, while GA is adept at local exploitation, refining solutions through crossover and mutation. By hybridizing these algorithms, it is possible to achieve a more balanced search process, combining the global exploration capabilities of FA with the local exploitation capabilities of GA. The hybrid approach can potentially improve convergence speed and solution quality. FA can guide the search toward promising regions of the solution space, while GA can refine these solutions further. This synergy can result in faster convergence to high-quality solutions compared to using either algorithm alone. Optimization problems in AI models, like tuning hyperparameters for SVR, often involve complex, multi-dimensional search spaces with multiple local optima. The hybrid method is well-suited for navigating such landscapes, as it combines the global search ability of GA with the local search refinement of FA (El-Shorbagy & El-Refaey, 2022; Mazen et al., 2016; Wahid et al., 2019; Wahid et al., 2019).

3. Results and discussion

3.1. Mathematical model validation

The mathematical model has been validated by (Forristall, 2003). The weather conditions and solar collector characterization in (Forristall, 2003) have been used as the input data. Table 3 depicts the performance of the mathematical model in terms of each component.

Table 3. Performance of the model by comparing the outcome and experimental data in (Forristall, 2003).

Variable	Ref. (Forristall, 2003)	Model	Relative error (%)
T_{outlet}	124	127.2	2.51
Effective heat (W/m)	3402	3470.2	1.96
Energy efficiency (%)	72.5	77.1	5.97

The maximum relative error is the energy efficiency, which equals 5.97%. This high relative error is mainly due to the high nonlinearity degree of the system.

3.2. Application of the recommended SVR model

Table 4. Continuous variables used for the optimization.

Factors	Unit	Lower bound	Upper bound
Inner diameter of the absorber tube	m	0.01	0.1
Distance between absorber tube and envelope	m	0.005	0.1
Length	m	1	150
Width	m	0.5	8
Mass flow	Kg/s	0.001	10
Pressure inside envelope	Pa	0	100,000
Initial temperature	°C	15	65

In this study, the SVR machine learning model is presented for solving nonlinear and complex problems in order to calculate economic metrics and assess environmental impacts. The model will be implemented in detail, and it can be applied to other complex projects as well. An example of the complexity of this study is dealing with a system of nonlinear equations and numerous variables. Time, energy, and money will be consumed in solving five nonlinear equations in order to derive the temperature profile. According to the solution, the CPU time for the solution of the main function is approximately 10 s. The optimization of a problem with 250 generations and a population of 200 takes approximately 138 h. The optimization time for this problem is high, as can be seen from the example. Minitab V 22.1 was used to generate the standard input data. The discrete and continuous factors were selected as 3 and 7, respectively (Table 4). By using Minitab software, 1500 input datasets were created. Then, by using computational code, all datasets were used as input, and a system of equations using these input data was solved. For the training of the SVR model, the sets of inputs and outputs were selected. The outputs include energy efficiency, exergy efficiency, heat cost, CO_2 emission cost based on energy, and CO_2 emission cost based on the exergy. The heat cost function includes cost function

($) and heat gain (*W*), which relate to energy efficiency. The input and output of the SVR model are depicted in Table 4 and Table 5. The input design is also depicted in Table 6.

Table 5. Discrete variables used for the optimization of the solar collector.

Working fluid	Gas inside the envelope	Material of absorber tube
Hitec XL	Air	Stainless steel 312
Water	Argon	Copper
Dowtherm Q	Hydrogen	Aluminium 2023
Therminol VP1		
Therminol TD12		
Therminol 72		

Table 6. Input design parameters and output of the model.

	Symbol	Unit	Description
Input	$D_{in,abs}$	m	Inner diameter of the absorber tube
	$R_{en\text{-}abs}$	m	Distance between absorber tube and envelope
	$\dot{m}$	Kg/s	Working fluid mass flow
	T_{in}	°C	Initial temperature of the working fluid
	L	m	Length of collector
	w	m	Width of collector
	P_{env}	Pa	Pressure inside of the envelope
	X_{abs}		Material of absorber tube
	X_{Wf}		Working fluid
	X_{env}		Gas inside the envelope
Output	η_{energy}	%	Energy efficiency
	η_{exergy}	%	Exergy efficiency
	C_H	$/kWh	Heat cost
	$CO_{2\text{-}energy}$	$	CO_2 emission cost
	$CO_{2\text{-}exergy}$	$	CO_2 emission cost

For the regression of the dataset, a Gaussian kernel was selected. ε was selected for optimization using the firefly algorithm with the characterization as in Table 7.

Table 7. Characterization of firefly algorithm for optimization.

Characterization	Description
Object of optimization	ε
Initial population	30
Iteration	50
Object function	Mean squared error (MSE)
Stop criteria	50^{th} iteration
Structure of fireflies	Based on the scale of the kernel

Figure 4 (a) illustrates the process of optimizing the SVR machine learning model. The MSE becomes constant after the 25th iteration of the optimization using the Firefly algorithm. Figure 4 (b) shows the regression results for all training, validation, and test data. According to the results, an ideal regression is obtained, and the regression number for the test data is 0.994. As well as using different methods to enhance accuracy, accuracy is primarily achieved by scaling input and output data to an appropriate range and applying nonlinear constraints to ensure meaningfulness. As a result of scaling data, large weights are not produced from the training model. An unstable model often exhibits high coefficient values, which may result in poor learning performance and sensitivity to input values, which may result in larger errors. Based on the analysis of the results, it is evident that there is a lack of data for regression for areas with nonlinear limitations on data generation. As a result, there are no data in this area, since these data are contradictory to reality and the fundamental physics of the problem. By following this approach, it is possible to avoid misdirection, incorrect training of machine learning algorithms, and the creation of unrealistic results. The optimization results are depicted in Figure 4 (c) by comparison between SVR and optimized SVR.

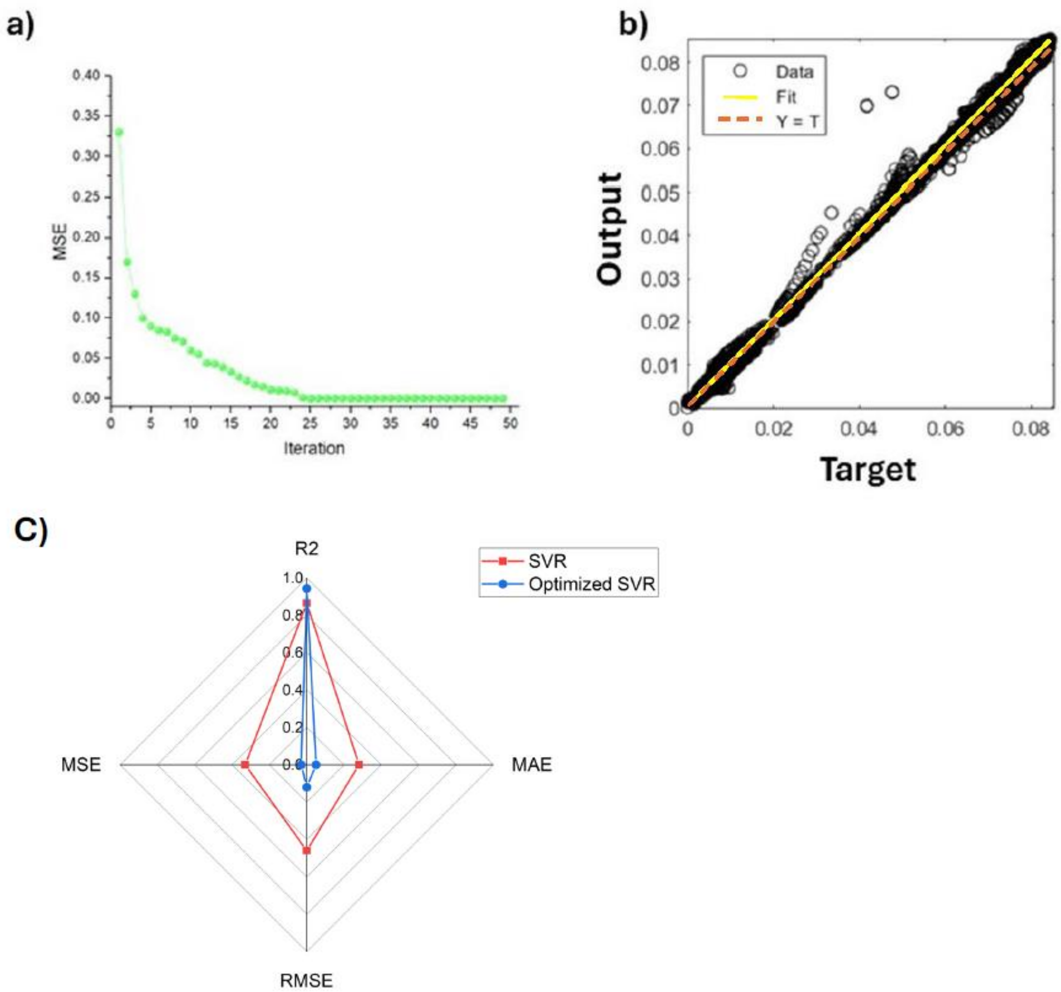

Figure 4. Performance of the SVR model: a) optimization procedure; b) results of the regression; c) comparison of performance and accuracy of the model before and after optimization.

3.3. Optimization

An effective and efficient way to provide accurate and appropriate machine learning models is to optimize and analyze the desired goals using different decision variables in order to solve the previously complex and time-consuming problem. Two object functions have been defined for the optimization of the design parameters of the system derived from the SVR model: exergy efficiency (%) and heat cost ($/kWh). As previously mentioned, the main reason for selecting the heat cost function was that it includes both the cost function ($) and the increase in useful heat gain (*W*), which are related to overall energy efficiency. In general, the optimization process aims to maximize exergy efficiency and minimize heat costs. Table 8 illustrates the main parameters of the genetic algorithm used in this study to optimize design parameters. The SVR model has the advantage of reducing the optimization process.

Table 8. Characterization of the genetic algorithm for optimization of design parameters.

Characterization	Multi-objective genetic algorithm
Decision-making variables	10
Population	200
Crossover	0.6
Mutation operator	adaptfeasible
Exchange function	Intermediate
Selection function	tournament
Accuracy	10^{-4}
Generation	250
Optimization time	5.1 min

Figure 5 illustrates the Pareto front, which indicates the two objective functions derived from the trained model. In accordance with the Pareto front, exergy efficiency increases as the heat cost function increases. Since energy efficiency decreases with an increase in exergy efficiency, which increases the cost function, there is an ideal point in the Pareto front that cannot be reached, but the optimal point is the closest to the ideal point.

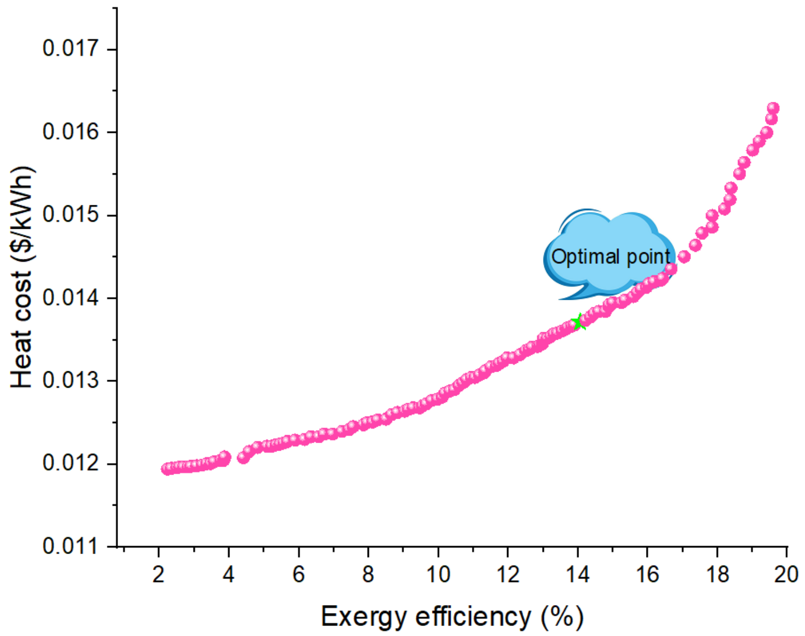

Figure 5. Pareto front for two optimization functions: heat cost and exergy efficiency.

As a result, the optimum reachable point based on the optimized design is the exergy efficiency of 14.05% with a heat cost of 0.0137 $/kWh. The optimized design parameters are illustrated in Table 9.

Table 9. Optimized design parameters.

Optimized value	Unit	Optimized value
Inner diameter of the absorber tube	m	0.016
Distance between absorber tube and envelope	m	0.008
Working fluid mass flow	Kg/s	0.46
Initial temperature of the working fluid	°C	55.1
Length of collector	m	2.69
Width of collector	m	2.11
Pressure inside of the envelope	Pa	0
Material of absorber tube		Copper
Working fluid		Water
Gas inside the envelope		Argon

3.4. Relation between design parameters and economic metrics

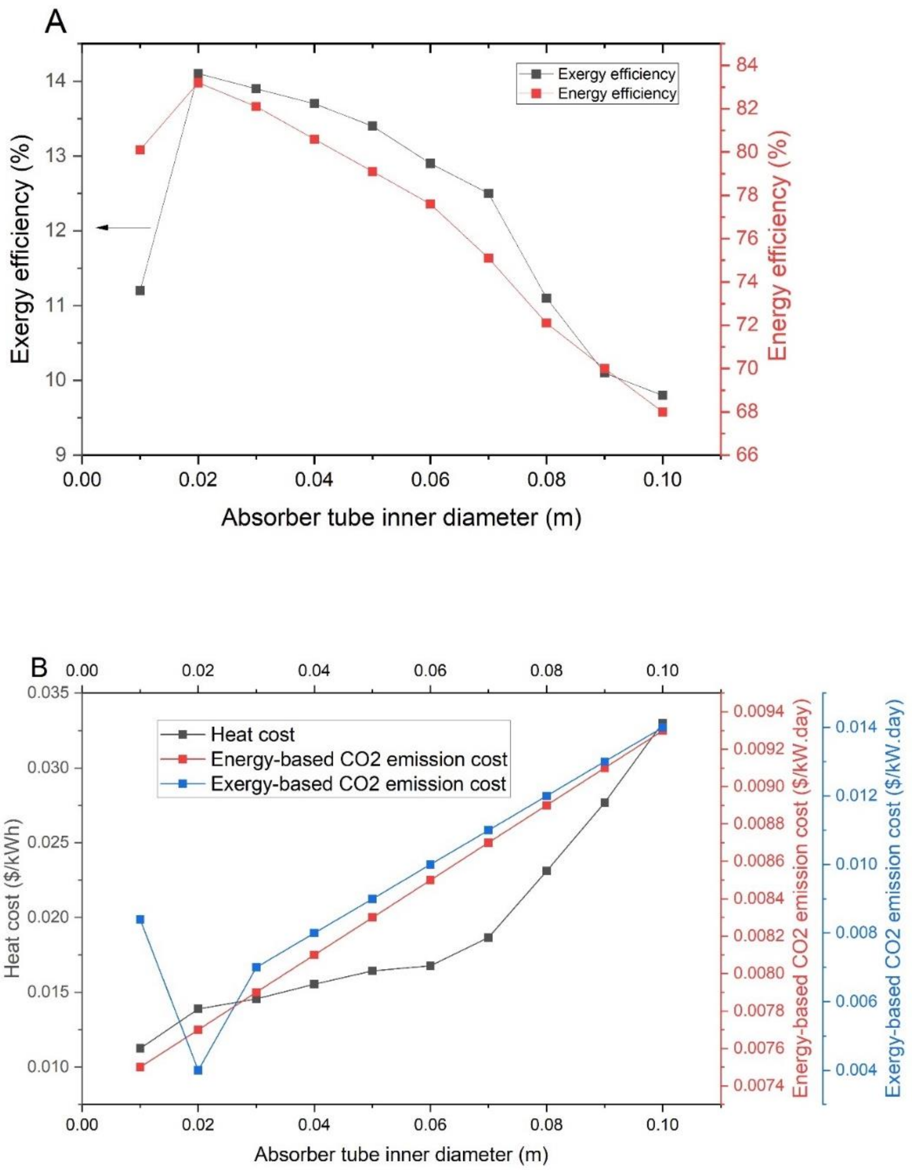

Figure 6. Effect of the inner diameter of the absorber tube on A) energy and exergy efficiencies, and B) heat cost-, energy-, and exergy-based CO_2 emission cost.

Figure 6 shows the energy efficiency, exergy efficiency, heat cost, and CO_2 emission cost based on energy and exergy according to the inner diameter. The heat cost will increase with an increase in diameter from 0.01 to 0.1 m. There is a descending trend in energy efficiency and exergy efficiency except for small diameters. Consequently, as the diameter decreases, both efficiencies will decrease. In small diameters, the pressure drop and the required power for pumping is high. As the diameter increases, the efficiency decreases due to a decrease in the Nusselt number and convection coefficient, which results in less heat being generated and more exergy being destroyed. So, there is a maximum point for the energy and exergy efficiencies when the inner diameter varies depending on whether the pressure drop or Nusselt number effect is dominant.

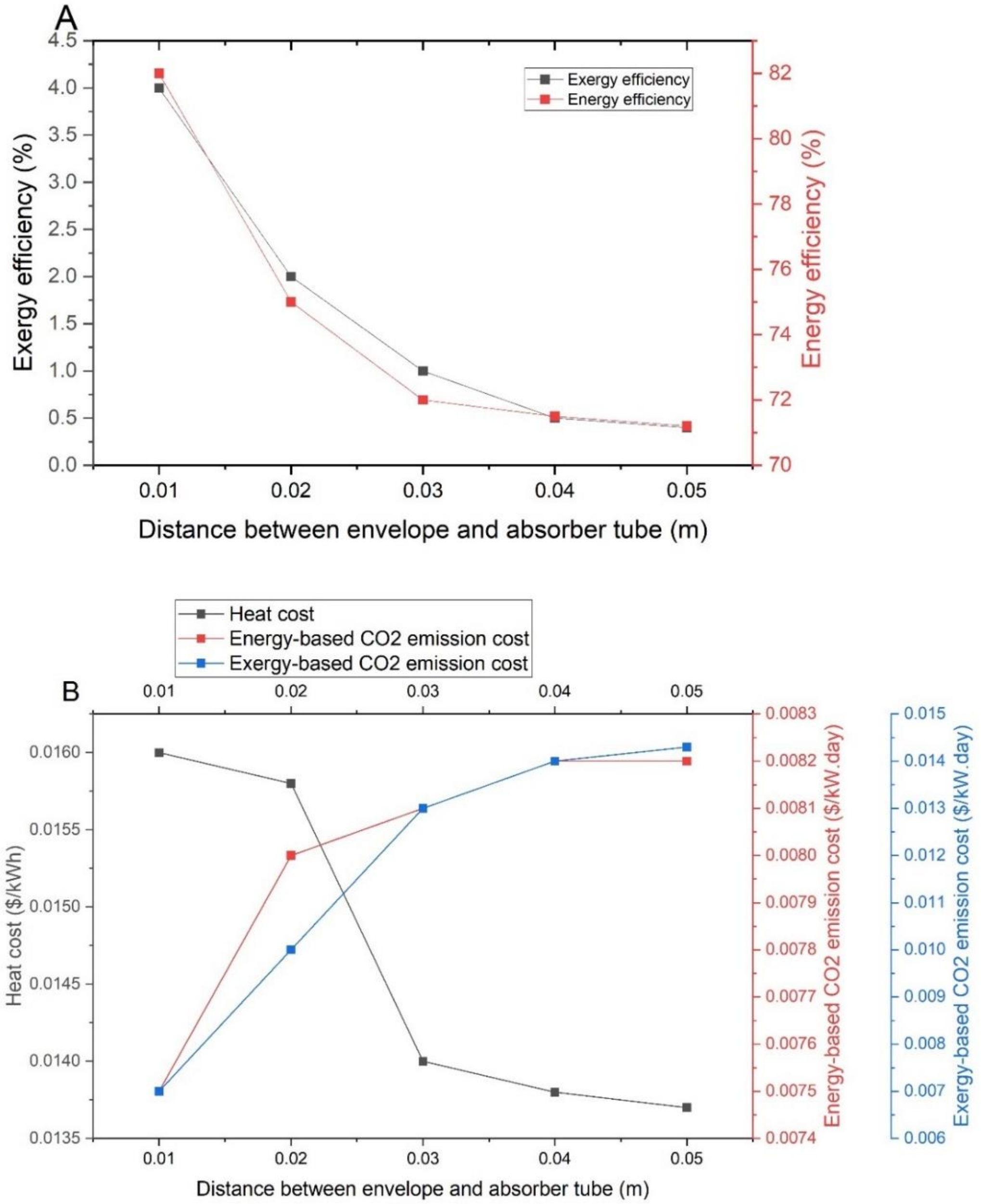

Figure 7. Effect of distance between the envelope and absorber tube on A) energy and exergy efficiencies, and B) Heat cost-, energy-, and exergy-based CO_2 emission cost.

It is necessary to provide a gap between the tubular absorber and the metallic reflector in order to prevent conduction heat loss from the absorber to the reflector and to provide a glass envelope around the absorber, which will increase the thermal efficiency of the compound parabolic concentrator (CPC) module at high temperatures. As a result of the gap between the absorber and the envelope, light incident on the absorber is lost, which is referred to as “gap losses”. It is therefore necessary a compromise between optical and thermal performance. Figure 7 depicts energy efficiency, exergy efficiency, heat cost, and CO_2 emission cost based on the energy and exergy efficiency vs. distance between absorber and envelope. With an increase in the distance from 0.01 to 0.05 m, the energy and exergy efficiencies will decrease due to the increase of convection heat transfer in annulus space.

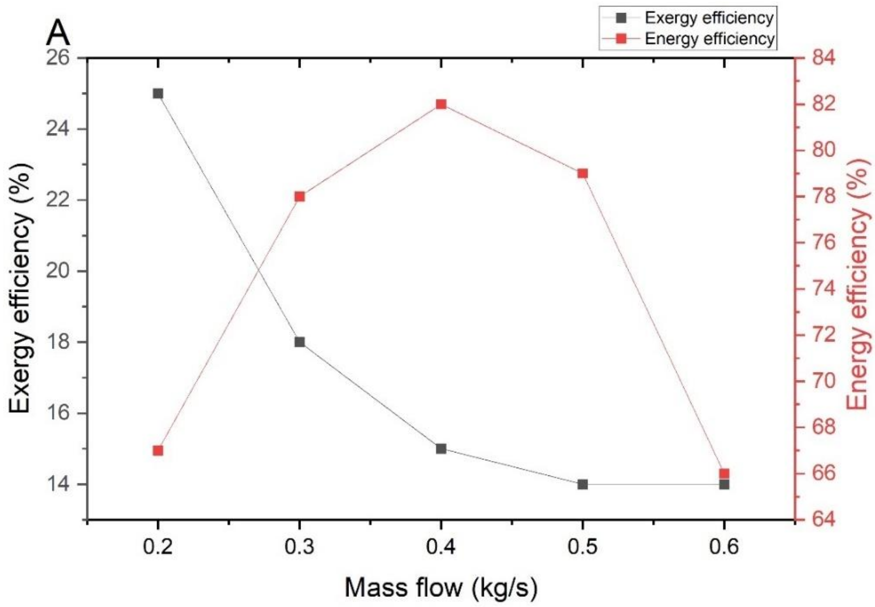

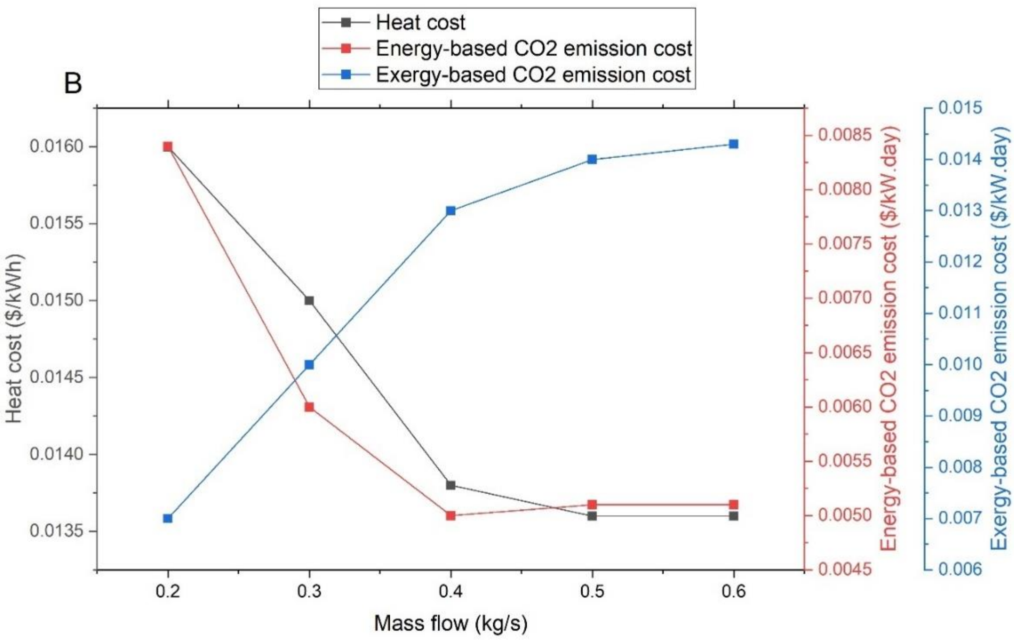

Figure 8. Effect of mass flow of working fluid on A) energy and exergy efficiencies, and B) heat cost-, energy-, and exergy-based CO_2 emission cost.

Figure 8 illustrates the effect of working fluid mass flow on efficiency and economic parameters. The increase in the mass flow will result in an exergy efficiency decrease. There is a maximum point for energy efficiency when mass flow rises. By increasing the mass flow by more than 0.2 kg/s, energy efficiency will decrease because of the lower heat transfer. The higher speed of the working fluid decreases the residence time of volume control of fluid inside the collector; therefore, the heat transfer and output temperature will decrease. In this analysis, energy efficiency is influenced by two main parameters: pressure drop and heat transfer coefficient. With the increase of mass flow rate, both increase; at a low mass flow rate, the convective heat transfer coefficient is dominant. However, energy efficiency is first upward and then downward. The cost of carbon dioxide emission based on energy and the cost of carbon dioxide emission based on exergy is shown as a function of the previously presented parameters.

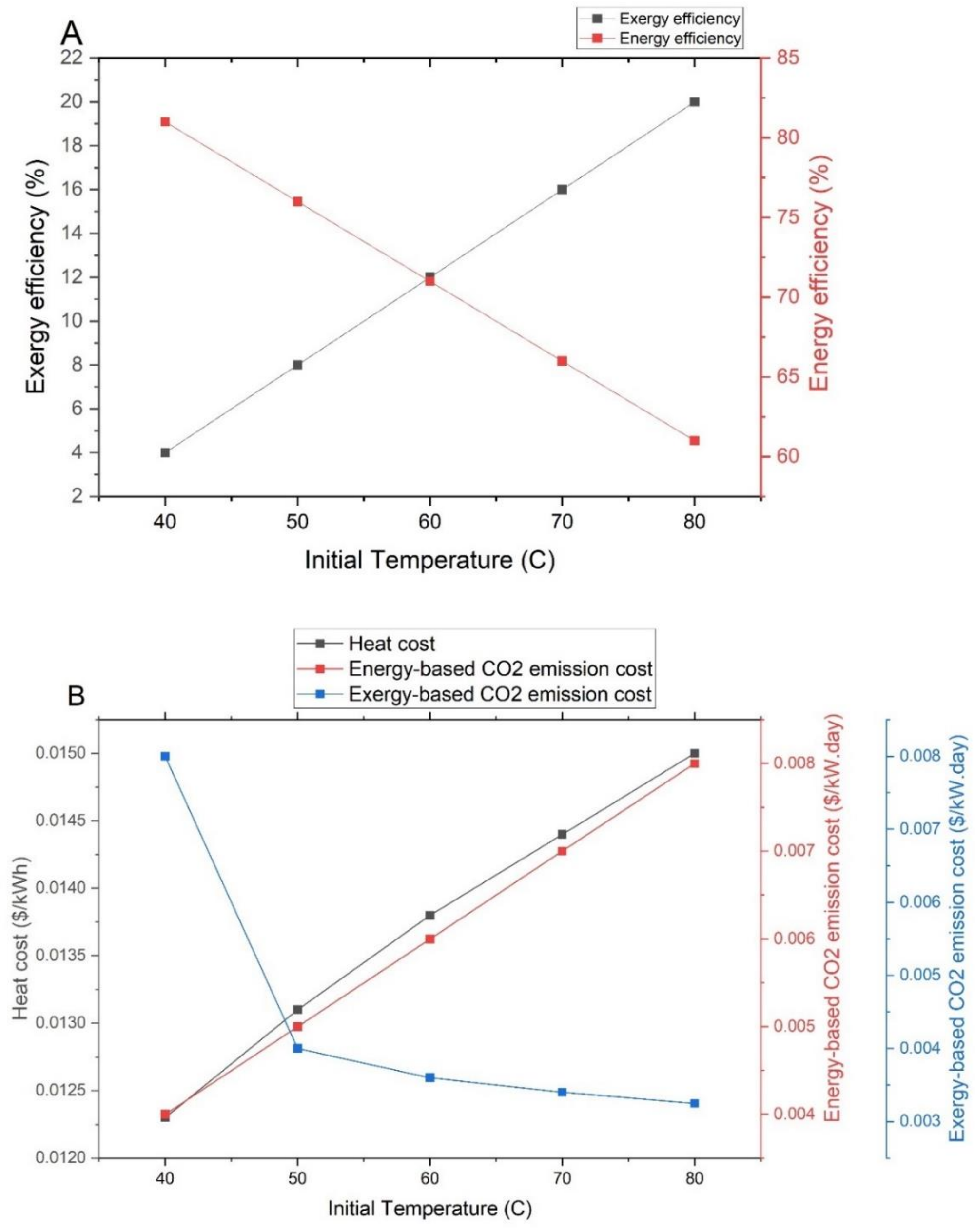

Figure 9. Effect of the initial temperature of working fluid on A) energy and exergy efficiencies, and B) heat cost-, energy-, and exergy-based CO_2 emission cost.

Based on Figure 9, with an increase in the inlet temperature, the energy efficiency decreases because the temperature difference between the fluid and the ambient environment decreases, resulting in a rise in the cost of heat. A temperature gap between hot and cold sources contributes to exergy destruction. By reducing the temperature difference, exergy destruction is reduced, which increases exergy efficiency.

3.5. Sensitivity analysis

Based on the trained model, a sensitivity analysis of all continuous and discrete variables was performed using the proposed machine learning approach. The sensitivity analysis was carried out based on the one factor at a time (OFAT) methodology. Based on the ±10% change in the design parameters, the percentage of change in energy efficiency, exergy efficiency, and heat cost was calculated. As can be seen from Figure 10, the results indicate that the most important parameter is the initial temperature of the working fluid.

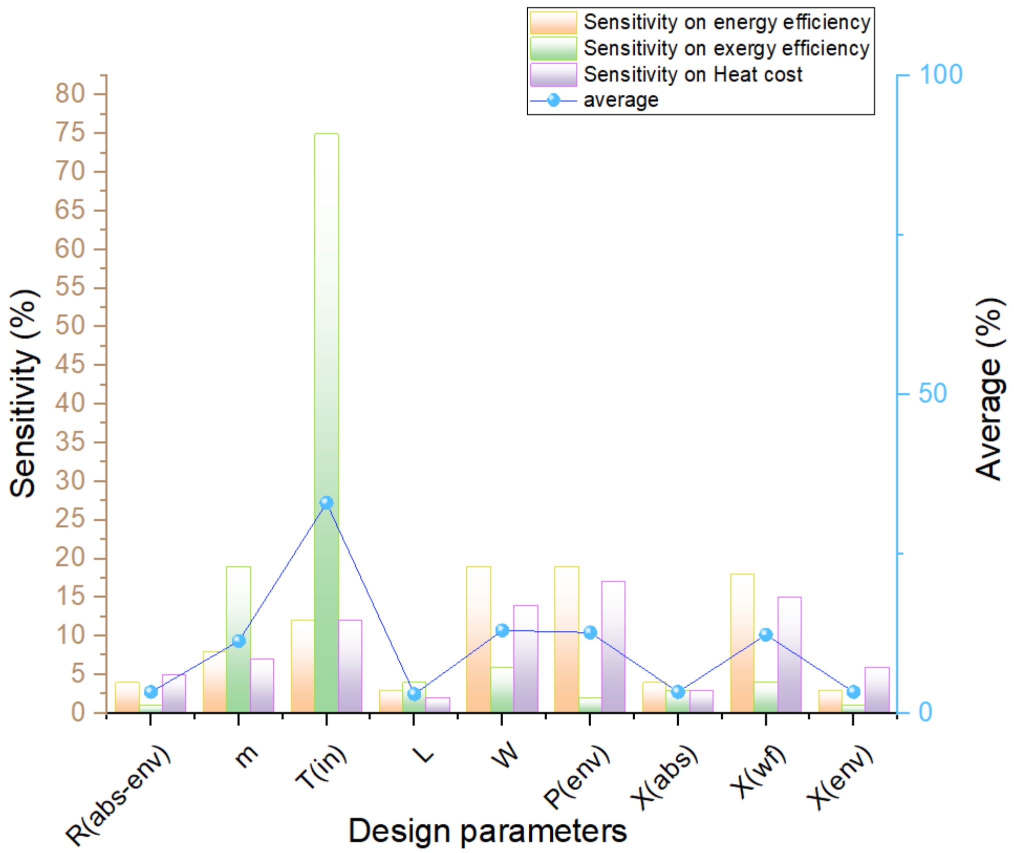

Figure 10. Sensitivity analysis of design parameters on energy efficiency, exergy efficiency, and heat cost.

3.6. Case study: Economic optimization of a solar collector in Calgary

In order to demonstrate the applicability of the proposed platform, a case study was developed to optimize a parabolic trough solar collector in Calgary (51.0447° N, 114.0719° W). Table 10 depicts the average monthly weather conditions with average solar irradiation.

Table 10. Monthly average of weather conditions in Calgary.

Month	Temperature (°C)	Wind speed (km/h)	Solar irradiation (kWh/m²/day)	Average sunlight (h/day)
January	−9.2	11.6	2.3	3.2
February	−4.1	13.8	3.2	4.1
March	−3.8	15.1	4.3	6.1
April	5.4	17.7	5.2	7.7
May	15.3	16.0	5.7	10.1
Jun	16.6	16.3	5.5	8.9
July	18.1	13.1	6.4	6.2
August	18.2	12.5	5.9	5.3
September	13.4	12.7	5.1	3.6
October	5.3	12.4	3.9	5.1
November	2.0	11.2	2.8	3.7
December	0.6	11.1	2.1	3.1

The platform was used to optimize the design of a parabolic trough solar collector and the optimum parameters for this system were determined (Table 11). As can be seen from Table 11, due to a higher average wind speed in Calgary, the average heat loss will be higher than the design parameters in Table 9. This resulted in a decrease in the distance between the envelope and the absorber tube. Therefore, the envelope cross-sectional area would be smaller, thereby decreasing forced convection heat transfer. Because the average number of sunny hours per day in (Forristall, 2003) is higher than in Calgary, the mass flow in the optimized design in Calgary was reduced, and the width of the collector was increased.

Table 11. Optimum design parameters for a solar collector located in Calgary, Alberta.

Optimized value	Unit	Optimized value
Inner diameter of the absorber tube	m	0.019
Distance between absorber tube and envelope	m	0.005
Working fluid mass flow	Kg/s	0.31
Initial temperature of the working fluid	°C	59.8
Length of collector	m	2.15
Width of collector	m	3.01
Pressure inside of the envelope	Pa	0
Material of absorber tube		Copper
Working fluid		Water
Gas inside the envelope		Argon

It is clear that the proposed platform can be used for optimizing the solar collector in each location based on the inputs and weather conditions. At optimum design parameters and operational conditions, the heat cost would be 0.0141 \$/kWh, and the levelized cost of gas generation would be 0.15 \$/kWh.

However, the expected levelized cost of renewable energy in Alberta is 0.05 $/kWh by 2035 (Ali, 2018; Barrington-Leigh & Ouliaris, 2017; Patel & Parkins, 2023).

4. Conclusions

In this comprehensive study, a support vector regression (SVR) algorithm was synergistically integrated with the firefly metaheuristic and genetic algorithms to forecast the economic profitability of solar power plants. Initially, mathematical modeling was employed to construct a robust dataset, which was subsequently utilized as the foundation for training the predictive model. Following the optimization of the SVR algorithm, the model was adeptly applied to evaluate the economic feasibility of the solar power plant. It was found that an increase in the inner diameter of the absorber tube was correlated with an escalation in heat costs, attributable to diminished energy and exergy efficiencies. Furthermore, it was observed that an increase in the distance between the envelope and the absorber tube resulted in a decline in heat cost, energy, and exergy efficiency, while paradoxically elevating CO_2 emission costs. An optimal heat transfer fluid flow rate of 0.4 kg/s was identified. Through sensitivity analysis, the paramount importance of the initial fluid temperature as a critical design parameter was underscored. Additionally, it was determined that the width of the collector and the pressure within the envelope space significantly influenced the leveled cost of energy.

In conclusion, the proposed hybrid optimization strategy was found to proficiently generate highly precise models, while concurrently fulfilling the objective of cost minimization. This methodology is considered to hold substantial promise for feasibility studies and conceptual design phases, offering a robust framework to evaluate the economic and environmental viability of energy projects prior to their construction.

Use of AI tools declaration

The authors declare they have not used Artificial Intelligence (AI) tools in the creation of this article.

Conflict of interest

The authors declare no conflict of interest.

References

Alawi OA, Kamar HM, Abdelrazek AH, et al. (2024) Design optimization of solar collectors with hybrid nanofluids: An integrated ansys and machine learning study. *Sol Energ Mat Sol C* 271: 112822. https://doi.org/https://doi.org/10.1016/j.solmat.2024.112822

Alawi OA, Kamar HM, Salih SQ, et al. (2024) Development of optimized machine learning models for predicting flat plate solar collectors thermal efficiency associated with Al2O3-water nanofluids. *Eng Appl Artif Intel* 133: 108158. https://doi.org/https://doi.org/10.1016/j.engappai.2024.108158

Ali B (2018) Forecasting model for water-energy nexus in Alberta, Canada. *Water-Energy Nexus* 1: 104–115. https://doi.org/10.1016/j.wen.2018.08.002

Ashouri M, Khoshkar Vandani AM, Mehrpooya M, et al. (2015) Techno-economic assessment of a Kalina cycle driven by a parabolic Trough solar collector. *Energ Convers Manage* 105: 1328–1339. https://doi.org/https://doi.org/10.1016/j.enconman.2015.09.015

Azad Gilani H, Hoseinzadeh S (2021) Techno-economic study of compound parabolic collector in solar water heating system in the northern hemisphere. *Appl Therm Eng* 190: 116756. https://doi.org/https://doi.org/10.1016/j.applthermaleng.2021.116756

Badescu V (2018) How much work can be extracted from diluted solar radiation? *Sol Energy* 170: 1095-1100. https://doi.org/10.1016/j.solener.2018.05.094

Barrington-Leigh C, Ouliaris M (2017) The renewable energy landscape in Canada: a spatial analysis. *Renew Sust Energ Rev* 75: 809–819.

Bellos E, Tzivanidis C (2017) A detailed exergetic analysis of parabolic trough collectors. *Energ Convers Manage* 149: 275–292.

Bergman TL (2011) *Fundamentals of heat and mass transfer*. John Wiley & Sons.

Brenner A, Kahn J, Hirsch T, et al. (2023) Soiling determination for parabolic trough collectors based on operational data analysis and machine learning. *Sol Energy* 259: 257–276. https://doi.org/https://doi.org/10.1016/j.solener.2023.05.008

Cuce PM, Cuce E (2023) Performance analysis of fresnel lens driven hot water/steam generator for domestic and industrial use: A CFD research. *Hittite J Sci Eng* 10: 1–9. https://doi.org/10.17350/HJSE19030000285

Cuce PM, Cuce E, Guclu T, et al. (2021) Energy saving aspects of green facades: Current applications and challenges. *Green Build Constr Econ* 2021: 18–28. https://doi.org/10.37256/gbce.2220211007

Cuce PM, Guclu T, Cuce E (2024) Design, modelling, environmental, economic and performance analysis of parabolic trough solar collector (PTC) based cogeneration systems assisted by thermoelectric generators (TEGs). *Sustain Energy Techn* 64: 103745. https://doi.org/https://doi.org/10.1016/j.seta.2024.103745

Deniz E, Çınar S (2016) Energy, exergy, economic and environmental (4E) analysis of a solar desalination system with humidification-dehumidification. *Energ Convers Manage* 126: 12–19. https://doi.org/10.1016/j.enconman.2016.07.064

Desai NB, Pranov H, Haglind F (2021) Techno-economic analysis of a foil-based solar collector driven electricity and fresh water generation system. *Renew Energy* 165: 642–656. https://doi.org/https://doi.org/10.1016/j.renene.2020.11.043

Duffie JA, Beckman WA, Blair N (2020) *Solar engineering of thermal processes, photovoltaics and wind*. John Wiley & Sons.

El-Shorbagy MA, El-Refaey AM (2022) A hybrid genetic–firefly algorithm for engineering design problems. *J Comput Des Eng* 9: 706–730. https://doi.org/10.1093/jcde/qwac013

Elfeky KE, Wang Q (2023) Techno-environ-economic assessment of photovoltaic and CSP with storage systems in China and Egypt under various climatic conditions. *Renew Energy* 215: 118930. https://doi.org/https://doi.org/10.1016/j.renene.2023.118930

Elsheikh A, Zayed M, Aboghazala A, et al. (2024) Innovative solar distillation system with prismatic absorber basin: Experimental analysis and LSTM machine learning modeling coupled with great wall construction algorithm. *Process Saf Environ Prot* 186: 1120–1133. https://doi.org/https://doi.org/10.1016/j.psep.2024.04.063

Faizal M, Saidur R, Mekhilef S, et al. (2015) Energy, economic, and environmental analysis of a flat-plate solar collector operated with SiO_2 nanofluid. *Clean Technol Envir* 17: 1457–1473. https://doi.org/10.1007/s10098-014-0870-0

Fister I, Fister Jr I, Yang XS, et al. (2013) A comprehensive review of firefly algorithms. *Swarm Evol Comput* 13: 34–46. https://doi.org/10.1016/j.swevo.2013.06.001

Forristall R (2003) *Heat transfer analysis and modeling of a parabolic trough solar receiver implemented in engineering equation solver*.

Frangopoulos CA (1987) Thermo-economic functional analysis and optimization. *Energy* 12: 563–571.

García-García JC, Ponce-Rocha JD, Marmolejo-Correa D, et al. (2019) Exergy analysis for energy integration in a bioethanol production process to determine heat exchanger networks feasibility. In A. A. Kiss, E. Zondervan, R. Lakerveld, & L. Özkan (Eds.), *Computer Aided Chemical Engineering*, 46: 475–480. Elsevier. https://doi.org/https://doi.org/10.1016/B978-0-12-818634-3.50080-1

Gnielinski V (1976) New equations for heat and mass transfer in turbulent pipe and channel flow. *Int J Chem Eng* 16: 359–367.

Haykin S (1998) *Neural networks: a comprehensive foundation*. Prentice Hall PTR.

Jehring L (1992) Bejan, A., Advanced Engineering Thermodynamics. New York etc., John Wiley & Sons 1988. XXIII, 758. ISBN 0-471-83043-7, Wiley Online Library.

Johari NF, Zain AM, Noorfa MH, et al. (2013) Firefly algorithm for optimization problem. *Appl Mech Mater* 421: 512–517.

Kalogirou SA (2004) Solar thermal collectors and applications. *Prog Energ Combust Sci* 30: 231–295. https://doi.org/10.1016/j.pecs.2004.02.001

Kottala RK, Balasubramanian KR, Jinshah BS, et al. (2023) Experimental investigation and machine learning modelling of phase change material-based receiver tube for natural circulated solar parabolic trough system under various weather conditions. *J Therm Anal Calorim* 148: 7101–7124. https://doi.org/10.1007/s10973-023-12219-9

Landsberg P, Mallinson J (1976) Thermodynamic constraints, effective temperatures and solar cells. International Conference on Solar Electricity.

Mazen F, AbulSeoud RA, Gody AM (2016) Genetic algorithm and firefly algorithm in a hybrid approach for breast cancer diagnosis. *Int J Comput Trends Tech* 32: 62–68.

Mehdipour R, Baniamerian Z, Golzardi S, et al. (2020) Geometry modification of solar collector to improve performance of solar chimneys. *Renew Energy* 162: 160–170. https://doi.org/https://doi.org/10.1016/j.renene.2020.07.151

Mustafa J, Alqaed S, Sharifpur M (2022) Numerical study on performance of double-fluid parabolic trough solar collector occupied with hybrid non-Newtonian nanofluids: Investigation of effects of helical absorber tube using deep learning. *Eng Anal Bound Elem* 140: 562–580. https://doi.org/https://doi.org/10.1016/j.enganabound.2022.04.033

Nguyen HM, Omidkar A, Li W, et al. (2023) Non-thermal plasma assisted catalytic nitrogen fixation with methane at ambient conditions. *Chem Eng J* 471: 144748. https://doi.org/https://doi.org/10.1016/j.cej.2023.144748

Omidkar A, Alagumalai A, Li Z, et al. (2024) Machine learning assisted techno-economic and life cycle assessment of organic solid waste upgrading under natural gas. *Appl Energy* 355: 122321. https://doi.org/https://doi.org/10.1016/j.apenergy.2023.122321

Omidkar A, Haddadian K, Es'haghian R, et al. (2024) Novel energy efficient in-situ bitumen upgrading technology to facilitate pipeline transportation using natural gas: Sustainability evaluation using a new hybrid approach based on fuzzy multi-criteria decision-making tool and techno-economic and life cycle assessment. *Energy* 297: 131280. https://doi.org/https://doi.org/10.1016/j.energy.2024.131280

Omidkar A, Xu H, Li Z, et al. (2023) Techno-economic and life cycle assessment of renewable diesel production via methane-assisted catalytic waste cooking oil upgrading. *J Clean Prod* 414: 137512. https://doi.org/https://doi.org/10.1016/j.jclepro.2023.137512

Pal RK, K RK (2021) Investigations of thermo-hydrodynamics, structural stability, and thermal energy storage for direct steam generation in parabolic trough solar collector: A comprehensive review. *J Clean Product* 311: 127550. https://doi.org/https://doi.org/10.1016/j.jclepro.2021.127550

Patel S, Parkins JR (2023) Assessing motivations and barriers to renewable energy development: Insights from a survey of municipal decision-makers in Alberta, Canada. *Energy Rep* 9: 5788–5798.

Pourasl HH, Barenji RV, Khojastehnezhad VM (2023) Solar energy status in the world: A comprehensive review. *Energy Rep* 10: 3474–3493. https://doi.org/https://doi.org/10.1016/j.egyr.2023.10.022

Ruiz-Moreno S, Sanchez AJ, Gallego AJ, et al. (2022) A deep learning-based strategy for fault detection and isolation in parabolic-trough collectors. *Renew Energy* 186: 691–703. https://doi.org/https://doi.org/10.1016/j.renene.2022.01.029

Salari A, Shakibi H, Soltani S, et al. (2024) Optimization assessment and performance analysis of an ingenious hybrid parabolic trough collector: A machine learning approach. *Appl Energy* 353: 122062. https://doi.org/https://doi.org/10.1016/j.apenergy.2023.122062

Shafieian A, Parastvand H, Khiadani M (2020) Comparative and performative investigation of various data-based and conventional theoretical methods for modelling heat pipe solar collectors. *Sol Energy* 198: 212–223. https://doi.org/https://doi.org/10.1016/j.solener.2020.01.056

Shboul B, Zayed ME, Al-Tawalbeh N, et al. (2024) Dynamic numerical modeling and performance optimization of solar and wind assisted combined heat and power system coupled with battery storage and sophisticated control framework. *Results Eng* 22: 102198. https://doi.org/https://doi.org/10.1016/j.rineng.2024.102198

Shboul B, Zayed ME, Tariq R, et al. (2024) New hybrid photovoltaic-fuel cell system for green hydrogen and power production: Performance optimization assisted with Gaussian process regression method. *Int J Hydrogen Energ* 59: 1214–1229. https://doi.org/https://doi.org/10.1016/j.ijhydene.2024.02.087

Sultan AJ, Hughes KJ, Ingham DB, et al. (2020) Techno-economic competitiveness of 50 MW concentrating solar power plants for electricity generation under Kuwait climatic conditions. *Renew Sust Energ Rev* 134: 110342. https://doi.org/10.1016/j.rser.2020.110342

Tabarhoseini SM, Sheikholeslami M, Said Z (2022) Recent advances on the evacuated tube solar collector scrutinizing latest innovations in thermal performance improvement involving economic and environmental analysis. *Sol Energ Mat Sol C* 241: 111733. https://doi.org/https://doi.org/10.1016/j.solmat.2022.111733

Vakili M, Salehi SA (2023) A review of recent developments in the application of machine learning in solar thermal collector modelling. *Environ Sci Pollut Res* 30: 2406–2439. https://doi.org/10.1007/s11356-022-24044-y

Vapnik VN (1999) An overview of statistical learning theory. *Ieee T Neural Networ* 10: 988–999.

Wahid F, Alsaedi AKZ, Ghazali R (2019) Using improved firefly algorithm based on genetic algorithm crossover operator for solving optimization problems. *J Intell Fuzzy Syst* 36: 1547–1562. https://doi.org/10.3233/JIFS-181936

Wahid F, Ghazali R, Ismail LH (2019) Improved firefly algorithm based on genetic algorithm operators for energy efficiency in smart buildings. *Arab J Sci Eng* 44: 4027–4047. https://doi.org/10.1007/s13369-019-03759-0

Wang Y, Kandeal AW, Swidan A, et al. (2021) Prediction of tubular solar still performance by machine learning integrated with Bayesian optimization algorithm. *Appl Therm Eng* 184: 116233. https://doi.org/https://doi.org/10.1016/j.applthermaleng.2020.116233

Wu S, Wang C, Tang R (2022) Optical efficiency and performance optimization of a two-stage secondary reflection hyperbolic solar concentrator using machine learning. *Renew Energy* 188: 437–449. https://doi.org/https://doi.org/10.1016/j.renene.2022.01.117

Yang XS (2010) Firefly algorithm, stochastic test functions and design optimisation. *Int J Bio-Inspir Com* 2: 78–84. https://doi.org/10.1504/IJBIC.2010.032124

Zayed ME, Aboelmaaref MM, Chazy M (2023a) Design of solar air conditioning system integrated with photovoltaic panels and thermoelectric coolers: Experimental analysis and machine learning modeling by random vector functional link coupled with white whale optimization. *Therm Sci Eng Prog* 44: 102051. https://doi.org/https://doi.org/10.1016/j.tsep.2023.102051

Zayed ME, Kabeel AE, Shboul B, et al. (2023b) Performance augmentation and machine learning-based modeling of wavy corrugated solar air collector embedded with thermal energy storage: Support vector machine combined with Monte Carlo simulation. *J Energy Storage* 74: 109533. https://doi.org/https://doi.org/10.1016/j.est.2023.109533

Zayed ME, Zhao J, Li W, et al. (2021) Predicting the performance of solar dish Stirling power plant using a hybrid random vector functional link/chimp optimization model. *Solar Energy* 222: 1–17. https://doi.org/https://doi.org/10.1016/j.solener.2021.03.087

AIMS Press

© 2024 the Author(s), licensee AIMS Press. This is an open access article distributed under the terms of the Creative Commons Attribution License (https://creativecommons.org/licenses/by/4.0)